Academic Journal of Science and Technology
ISSN: 2771-3032 | Vol. 10, No. 1, 2024

Numerical Simulation-Based Study on the Microstructure of TC4 Titanium Alloy in CMT Additive Manufacturing

Jiaxing Guo

School of Nanchang Hangkong University, Guangzhou 330000, China

Abstract: This thesis explores the thermal and mechanical phenomena occurring during the Cold Metal Transfer (CMT) additive manufacturing process of TC4 titanium alloy. The investigation delves into the effects of layer-by-layer deposition on the thermal cycles, stress distribution, and microstructural evolution of the additive manufactured specimens. Key findings include the identification of thermal accumulation with increasing deposition layers, leading to a decrease in cooling rates and a slight increase in the peak molten pool temperatures. The temperature profiles on the substrate exhibit cyclic patterns of peaks and troughs, which become smoother and exhibit less variance between maximum and minimum temperatures as deposition progresses. Stress analysis reveals that equivalent stress within the deposited layers decreases with the number of layers. This is attributed to the thermal stress accumulation and stress cycles induced by multiple thermal cycles, which initially increase the equivalent stress. However, a reduction in cooling rates over time and the effects of remelting facilitate the release of interlayer stress, resulting in minimal residual stress within the cooled specimens. Microstructurally, the TC4 titanium alloy specimens are characterized by the presence of primary β phase spanning across multiple deposition layers, growing in the direction of additive manufacturing. The accumulated heat input from increased layering enhances the growth of the primary β phase.The specimens' microstructure features a basketweave pattern comprised of α', α, and β phases, with α' martensite directly transformed from the primary β phase. Repeated heating cycles foster diverse pathways for the secondary α phase's formation, leading to more pronounced, directionally parallel α phases and extensive basketweave structures within the specimen layers. Higher temperature gradients at specimen edges encourage the formation of needle-like α' martensite. This thesis contributes to the understanding of the thermal behavior, stress dynamics, and microstructural characteristics in TC4 titanium alloy during CMT additive manufacturing, highlighting the interplay between process parameters, thermal management, and material response.

Keywords: TC4 titanium alloy; microstructure evolution; numerical simulation.

1. Introduction

Titanium alloys, particularly TC4 (Ti-6Al-4V), have garnered extensive attention in various high-performance engineering applications ranging from the aerospace to the biomedical sectors[1]. These alloys are celebrated for their exceptional blend of mechanical properties, corrosion resistance, and high-temperature durability. Among the fabrication techniques available, Additive Manufacturing (AM) stands out for its ability to intricately craft components with complex geometries, minimal waste, and tailored properties[2,3]. Within the realm of AM, the Cold Metal Transfer (CMT) method emerges as a particularly promising technique for TC4 titanium alloy, characterized by its low heat input and stable arc, which are pivotal for reducing thermal-induced stress and distortion[4].

Despite the promising attributes of CMT for additive manufacturing of TC4 alloys, several challenges impede its widespread adoption. One of the primary hurdles is the control of microstructure and residual stresses during the manufacturing process, which significantly influence the final mechanical properties of the fabricated parts[5]. The intricate interplay between the rapid cooling rates and the thermal gradient inherent in CMT processes necessitates a profound understanding and optimization to mitigate defects and enhance material performance[6].

In this context, numerical simulation presents itself as an invaluable tool for preemptively identifying and addressing potential issues within the AM process. Through simulating the temperature and stress fields, researchers can gain insights into the thermal behavior, residual stress evolution, and subsequent microstructural developments during AM[7]. The utilization of SYSWELD software for these purposes enables the detailed investigation of the CMT process applied to TC4 alloys, offering a pathway to optimize parameters for improved outcomes[8].

However, a noticeable gap exists in the literature regarding the comprehensive exploration of how temperature and stress fields specifically influence the microstructure of CMT additive manufactured TC4 titanium alloy. This study aims to bridge this gap by employing numerical simulations to elucidate these relationships and conducting microstructural analysis to validate the simulated results. Through this approach, the research seeks to contribute valuable knowledge towards the optimization of CMT additive manufacturing processes for TC4 titanium alloy, paving the way for enhanced material properties and broader application potential[9].

2. Experimental Materials and Methods

2.1. Equipment & Materials

The experiment used TC4 titanium alloy as the material, with the substrate dimensions being 200 mm × 80 mm × 3 mm, and the filler wire material being Φ1.2 mm TC4 wire, the composition of which is the same as that of the substrate material. The main composition of the TC4 titanium alloy

substrate and filler wire material is shown in Table 1.

Table 1. The chemical component of TC4 alloys substrate and welding wire

Sort	Al	V	Fe	C	N	H	O	Ti
welding wire	6.05	4.00	0.15	0.02	0.01	0.003	0.018	Excess
substrate	6.10	3.90	0.15	0.02	0.05	0.015	0.02	Excess

The CMT additive manufacturing experiment utilized a Fronius TPS2700 CMT welding machine. The welding torch was fixedly mounted on a KUKA six-axis robotic arm. The process parameters for CMT additive manufacturing are shown in Table 2, where the welding heat input formula is:

$$E = \eta \frac{UI}{v} \quad (1)$$

Table 2. Processing parameters of CMT additive manufactured TC4 alloys thin wall

Wire feeding speed (m/min)	Welding speed (m/min)	current (A)	voltage (V)	Lift height (mm)	Amount of heat input (J/cm)
5.5	0.3	136	11.8	3.0	2567.7

where I represents the welding current (A); U represents the welding voltage (V); ν represents the welding speed (cm/s); and η represents the thermal efficiency coefficient (=0.8).

Samples were taken from the middle stable region of the thin-walled deposition layer of the TC4 titanium alloy after CMT arc additive manufacturing for observation. The extracted samples were mounted and polished step by step with sandpaper up to 5000#. The etchant used was Kroll's reagent.

2.2. Numerical simulation of CMT additive TC4 titanium alloy

2.2.1. Thermophysical properties of TC4 titanium alloy

With the increase of temperature, the thermophysical parameters (density, thermal conductivity, specific heat, thermal expansion rate) and mechanical property parameters (yield strength, elastic modulus) of TC4 titanium alloy will change to a large extent, so it is not appropriate to use the performance parameters of TC4 titanium alloy at room temperature to calculate the additive high temperature process. For example, the Poisson's ratio of TC4 titanium alloy in the material library does not change with time, so in order to make the simulation results more accurate, the thermophysical parameters of TC4 titanium alloy in the software are modified, as shown in Table 3.

Table 3. Thermal physical properties of TC4 Titanium alloy

temperature (℃)	Young's modulus GPa	Poisson's ratio	density kg/m3	Specific heat capacity J/kg·K	Thermal conductivity W/mK	Coefficient of thermal expansion 10-6/℃
20	113.8	0.32	4450	611	6.82	9.1
200	108.0	0.33	4430	653	8.74	9.2
400	100.0	0.33	4440	691	10.28	9.5
600	94.0	0.34	4370	713	13.72	10
1000	80.0	0.38	4320	754	18.29	11
1400	50.0	0.40	4250	787	24.52	11
1650	10.0	0.41	4190	805	22	11
1800	0.12	0.50	4000	806	20	11
2000	0.12	0.50	3930	980	21	11

2.2.2. Selection of CMT additive heat source model

The establishment of the CMT additive heat source model is a prerequisite for analyzing the additive thermal cycle process and molten pool behavior. Based on the mode of action, additive heat sources are divided into concentrated, planar distributed, and volumetric distributed types. During CMT welding, due to the large depth-to-width ratio of the weld bead and the significant influence of heat flow along the thickness direction of the workpiece, the heat source should be considered as one with a certain volumetric distribution. To account for the distribution of arc heat flow along the thickness direction of the workpiece, the volumetric distributed heat source can be described as an ellipsoidal mode (including hemispherical and double ellipsoidal). During CMT welding, the welding speed has a smaller impact on the pre-arc heating zone than on the post-arc heating zone, resulting in the heating zone being represented by a pair of hemispherical bodies, symmetrically arranged around the weld centerline, rather than a single hemispherical body. The shapes of the two hemispheres are different, thus, the volumetric heat source distribution acting on the workpiece is divided into front and rear sections. Assuming the double hemispheres as semi-axes, the heat flow distribution within the front and rear hemispheres can be represented as:

$$q_f(x,y,z) = \frac{6\sqrt{3}(f_f Q)}{a_f b_h c_h \pi\sqrt{\pi}} exp\left(-\frac{3x^2}{a_f^2} - \frac{3y^2}{b_h^2} - \frac{3z^2}{c_h^2}\right), x \geq$$

$$q_r(x,y,z) = \frac{6\sqrt{3}(f_r,Q)}{a_r b_h c_h \pi\sqrt{\pi}} exp\left(-\frac{3x^2}{a_r^2} - \frac{3y^2}{b_h^2} - \frac{3z^2}{c_h^2}\right), x < 0$$

where a_f , a_r , b_h , c_h are the shape parameters of the heat source; Q represents the heat input during welding,$Q=\eta UI$, in watts (W); η is the thermal efficiency; U is the welding voltage (V); I is the welding current (A); f_f,f_r are the front and rear energy distribution parameters, respectively, with $f_f+f_r=2$. Figure 1 shows the double ellipsoidal heat source model, where the heat source is symmetrical about the z-axis and moves along the y-axis during heat source loading.

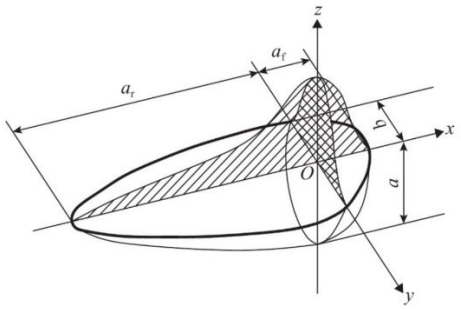

Figure 1. Thermal source of dual-ellipsoid

2.2.3. CMT additive model simplification, building, and meshing

The modeling was performed using SYSWELD software, and the finite element model of the additive specimen is shown in Figure 2. To maximally reproduce the working condition, modeling was carried out at a 1:1 scale with the real additive specimen, with the substrate dimensions being 200mm×100mm×2mm, and a single path of additive manufacturing was performed in the center of the substrate. During modeling, in areas with large temperature gradients (especially near the heat source), the mesh was divided more finely to achieve higher unit density; while in areas far from the heat source, due to smaller temperature gradients, the mesh was coarser to balance the speed and accuracy of the calculation. In this paper, the mesh was divided more finely in the central additive area of the substrate and the subsequent additive layers, slightly coarser near the central area of the substrate. Since the temperature gradient in the edge area of the substrate is smaller and it is not the main research target, the mesh was coarser to save on calculation time.

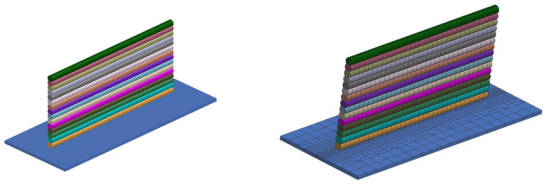

Figure 2. Finite element model

The CMT arc additive manufacturing process is not only a typical unstable nonlinear problem but also a very complex physicochemical process, making the solving process complicated. To improve the efficiency of the numerical simulation of the additive manufacturing process, some appropriate assumptions and simplifications were made in this study:

1. The ambient temperature during the experiment is 20°C;
2. The filling effect of the deposited metal is ignored;
3. The material is considered as a continuous medium and isotropic;
4. It is assumed that the molten pool fluid remains stationary during the welding process;
5. The deformation produced during the welding process is considered ideal elastoplastic;
6. The mechanical properties of the material obey the von Mises yield criterion;
7. The effect of creep is not considered during the welding process.

3. Experimental Results and Analysis

3.1. Simulation results of CMT additive temperature field

For the numerical simulation of the CMT arc additive process on TC4 titanium alloy, a single-track multi-layer deposition method was adopted. The process parameters were based on actual conditions as follows: welding voltage of 11.8 V, welding current of 136 A, wire feeding speed of 5.5 m/min, welding speed of 0.3 m/min, inter-layer cooling for 120s, and thermal efficiency of 0.6.

The simulation of the CMT arc additive process on TC4 titanium alloy with the above parameters showed results as depicted in Figure 3. The figure illustrates the transient temperature field distribution at different deposition layers when the heat source moves in the deposition direction. Influenced by the direction of the heat source movement, the metal temperature distribution behind the heat source presents a semi-ellipsoidal shape with a larger heated area, while the metal temperature distribution in front of the heat source is smaller. As the heat source moves in the welding direction, the shape of the isotherms remains essentially unchanged, gradually advancing forward. In Figure 3(a), at the center of the first layer of addition, the edge of the substrate remains at room temperature, while the temperature at the center of the heat source reaches up to 1700°C, indicating that the first layer of deposition experienced a process of melting followed by rapid solidification. In Figure 3(b), it can be observed that the molten pool significantly enlarges, and the previous deposition layer exhibits remelting, which is due to the extreme heat generated after several layers of CMT additive, resulting in an overall temperature increase and a reduced cooling rate. In Figure 3(c), the molten pool further enlarges, and the temperature of the previous deposition layer reaches above 500°C, which will have a preheating effect. In Figure 3(d), when adding to the last layer, the size of the molten pool reaches its maximum, and due to the multiple additions previously, the entire specimen is within a higher temperature range, and the previous deposition layers will experience multiple thermal cycles.

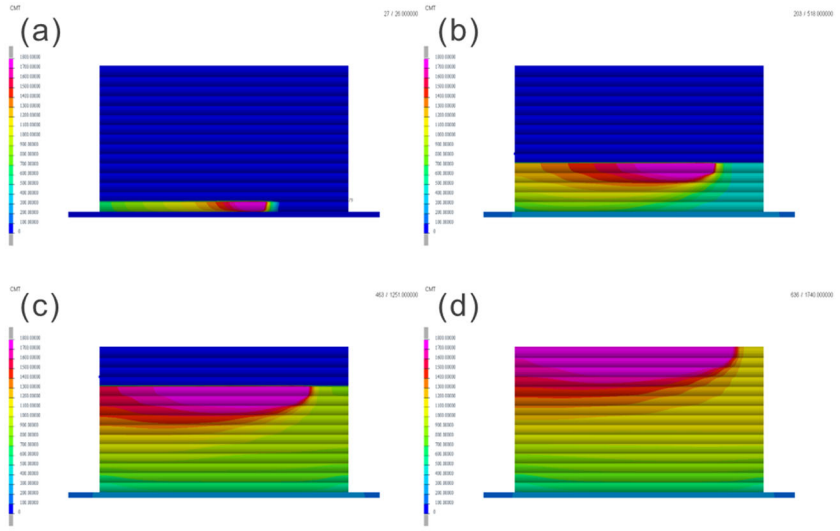

Figure 3. Distribution of transient temperature field

Figure 4 shows the thermal cycling at a point in the center of the first deposition layer during the multi-layer deposition process. It can be seen from the figure that when the point is passed during the first deposition, its temperature reaches a maximum of 2200°C. When the heat source passes above this point at the second deposition layer, the temperature at this point rapidly rises back to 1672°C, where the point is melted again and metallurgically merges with the second layer of welding; as the deposition process continues, the peak temperature at this point gradually decreases, and the temperature of the thermal cycling curve gradually rises in a fluctuating manner. The cooling phase curve becomes gradually smoother, nearing a smooth curve after the fifth thermal cycle, and the overall temperature tends to stabilize.

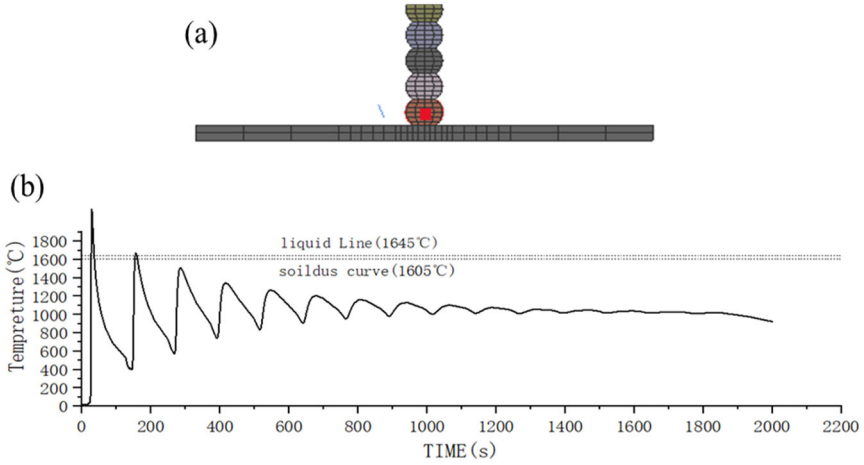

(a) Schematic diagram of the thermal cycle pick-up point; (b) Thermal cycling curves。

Figure 4. Thermal cycling curve at one point on the first sedimentary layer

3.2. Simulation results of CMT additive stress field and deformation

The stress field during the single-pass multi-layer CMT additive manufacturing process is influenced by many factors, such as heat input, cooling rate, and interlayer temperature, etc. Moreover, in the CMT additive manufacturing process, as the heat source moves along a specific path, it leads to an uneven distribution of the stress field within the component. The areas near the molten pool, having experienced higher temperatures, may exhibit significant stress concentration. Figure 5 shows the equivalent stress at different moments during the single-pass multi-layer CMT additive manufacturing process. It is evident from the figure that as the number of deposited layers increases, the equivalent stress on and around the deposited layers on the substrate gradually decreases, with the highest equivalent stresses for the first, fourth, and fifteenth layers being 375 MPa, 163 MPa, and 32 MPa, respectively. The stress contour maps show the largest equivalent stress distribution in the first deposition layer, which is because the cooling rate significantly affects the magnitude and distribution of residual stresses. Rapid cooling typically leads to larger residual tensile stresses, while a slower cooling rate facilitates the release and uniform distribution of stress. According to the results of the temperature field mentioned earlier, the first layer has the fastest cooling rate, hence the highest equivalent stress distribution. The stress contour maps also reveal that as the number of deposited layers increases, the overall equivalent stress of the specimen decreases. This is partly because, after depositing multiple layers, the overall temperature of the specimen rises, and the higher interlayer temperature can

reduce the accumulation of thermal stress, thereby lowering residual stress. On the other hand, the remelting phenomenon that occurs during the deposition process releases some of the internal equivalent stresses in the metal.

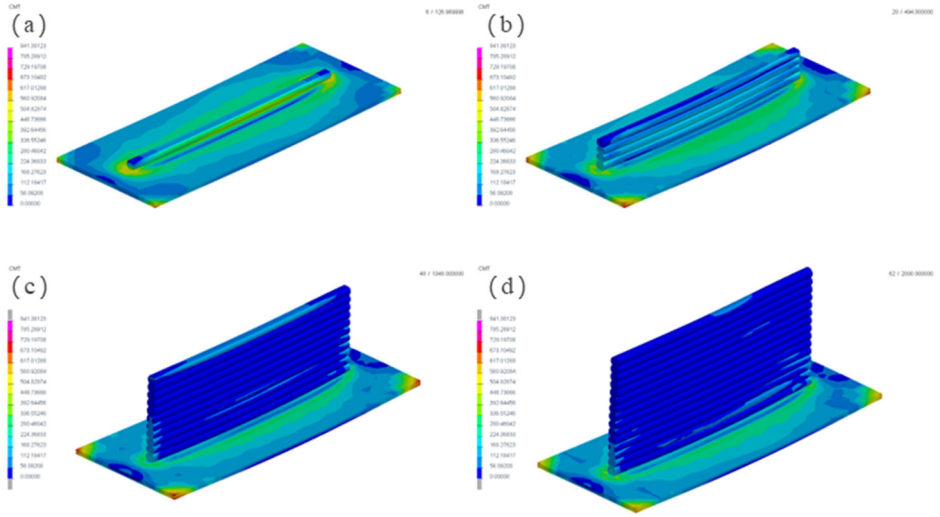

(a)The first course; (b)The fourth course; (c)Tenth course; (d)The fifteenth;

Figure 5. The equivalent stress distribution in the p rocess of multilayer stacking

To further investigate the equivalent stress conditions between deposition layers and the impact of deformation on the stress field, the CMT arc additive TC4 model was sectioned, as shown in Figure 6. From the figure, it can be seen that the deformation of the additive sample is essentially symmetrically distributed, mainly manifesting as the corners lifting, which is related to the position and form of the displacement constraints applied, consistent with the results in real production. In terms of stress, it is found that after the cooling process of each stacking, the equivalent stress state at the interlayer joint is less than that in other areas, also benefiting from the effect of remelting. After the addition is complete, the main stress concentration areas are at the two ends where the additive part connects with the substrate, primarily caused by deformation.

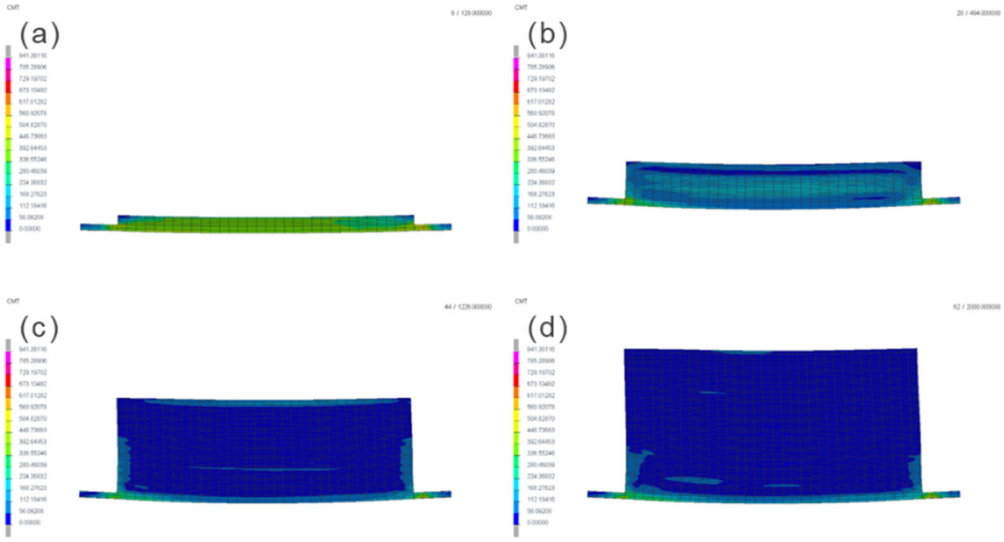

(a)The first course; (b)The fourth course; (c)Tenth course; (d)The fifteenth;

Figure 6. The equivalent stress distribution of the section during the multi-layer stacking process

3.3. Heat source checking

During the experimental process, a K-type thermocouple was connected to a multi-channel temperature recorder to measure and record temperatures. Before measuring, a hole was drilled on one side of the substrate so that the thermocouple, after being inserted, was positioned directly below the deposition layer. For temperature measurement, one end of the K-type thermocouple was embedded into the pre-drilled hole.

In the actual additive manufacturing process, the thermal cycling curve at a point on the substrate was measured using a K-type thermocouple. The thermal cycling curve obtained from the model at the same position was compared, as shown in Figure 7. Both thermal cycling curves, in terms of values and trends, were close to each other, within an acceptable error range. This indicates that the model established in this paper and the chosen heat source model are accurate

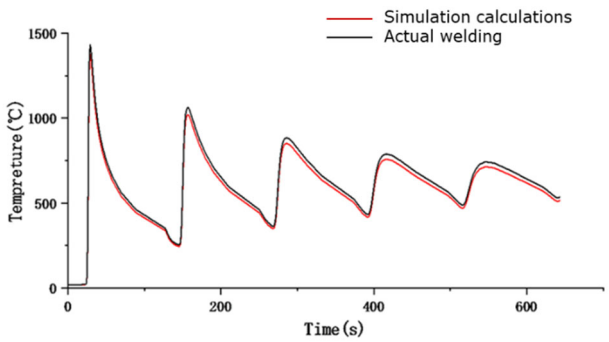

Figure 7. Calculated thermal cycle curve contrasting with measured curve

3.4. CMT additive TC4 titanium alloy structure

Figure 8 shows macroscopic cross-sectional photos of the deposition layers and a schematic of their locations. Due to the numerous deposition layers and large size of the specimen, it was divided into multiple parts for observation. The sampling locations are as shown in Figure 4-1, with samples (a)-(f) taken continuously from the bottom to the top.

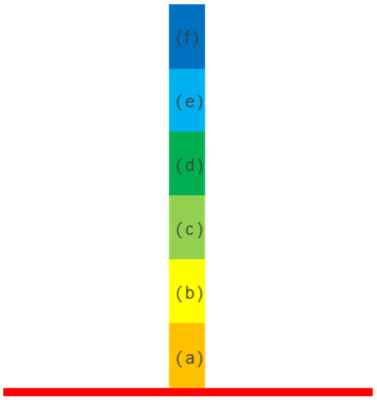

Figure 8. Schematic diagram of the position of the macro specimen

After cutting, the cross-section of the additive manufacturing specimen was polished, polished, and etched, and then observed under a macro lens camera, resulting in Figure 9. In the process of CMT arc additive manufacturing (TC4 titanium alloy), the interlayer fusion line between two continuous deposition layers was clearly observed, marked with a dashed line. Due to the accumulation of heat during the CMT AM process, the primary β phase was observed to penetrate several deposition layers and grow in the direction of addition. This phenomenon has also been found in other additive manufacturing technologies such as Selective Laser Melting (SLM), Electron Beam Melting (EBM), and Wire Arc Additive Manufacturing (WAAM). Despite the relatively low heat input of the CMT process, continuous layer-by-layer deposition still promoted the formation of coarser primary β phases. These coarse grains are known as original β grains, with their boundaries referred to as Solidification Grain Boundaries (SGB). Smaller equiaxed β grains, known as prior-β grains, are visible at the top and bottom of the sample, the starting point of which is defined as nucleation. The final size of an individual prior-β grain is determined by the number of nucleation points. As atoms are added sequentially, the grains gradually increase in size until they collide with neighboring growing grains. The interface between two contacting prior-β grains is also marked as a Solidification Grain Boundary (SGB). The columnar crystals at the bottom of the deposition layer grow in the direction of deposition. During the additive process, their growth direction changes, deviating from the original growth direction at a certain angle. This phenomenon results from the reduction of the temperature gradient during the additive process, with the columnar crystals tending to develop in the direction of fastest heat dissipation. The growth of prior-β columnar grains is mainly due to two reasons: firstly, the solidification temperature range of TC4 is very small (about 5 K), leading to rapid solidification of the early deposition layers. This means that when the previous deposition layer is heated to the liquidus temperature, the prior-β grains grow rapidly and continue to expand outward from the solidification front, forming coarser β grains in the early layers. The lower heat input and faster cooling rate together form a slender grain structure. Experiments indicate that merely reducing the heat input is not enough to prevent the formation of columnar crystals. Additionally, the formation of a few equiaxed crystals at the bottom and top of the specimen is mainly due to the high temperature gradient provided by the cooling baseplate at the bottom and the extremely fine equiaxed crystals constituting the TC4 baseplate itself, while the smaller columnar crystals at the top have a faster cooling rate due to their large surface area in contact with the external environment and are not affected by subsequent deposition layers.

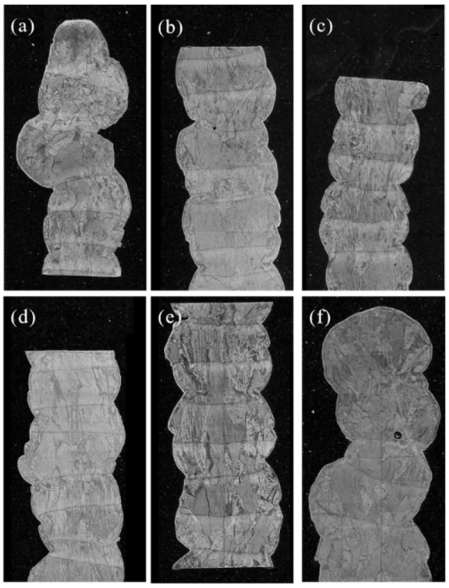

Figure 9. CMT additive TC4 titanium alloy macro structure CMT additive TC4 titanium alloy macro structure

At room temperature, the TC4 titanium alloy consists of the hexagonally close-packed α phase and the body-centered cubic β phase. During the CMT additive process, as the molten pool is heated, the local temperature of the material rises above the β transition temperature (the formation temperature of the β phase). At this point, the original α phase begins to transform into the β phase, forming a high-temperature stable β phase region. As the material cools, the β phase begins to transform back into the α phase. However, due to the rapid cooling rate of the CMT additive process, some of the β phase may be supercooled and retained, not completely transformed into the α phase, or forming a metastable α' martensite phase. Under rapid cooling conditions, the β phase may directly transform into the

metastable α' martensite phase. The α' martensite is a distorted hexagonal close-packed (HCP) structure, different from the original β body-centered cubic (BCC) structure, which increases the hardness and strength of the alloy but may sacrifice toughness. Although the heat input of the CMT process is relatively low, with the deposition of subsequent layers, the cooling rate decreases and thermal accumulation becomes severe, the microstructure in the bottom area will change due to the effect of the thermal cycle, which may include coarsening of the α phase and redistribution of the β phase.

The microstructure at the top section of the TC4 titanium alloy CMT arc additive specimen is shown in Figure 10(a), featuring a typical basketweave structure. The basketweave structure is composed of numerous slender α phases crisscrossing each other. Because the topmost deposition layer lacks continuous heat input and cools rapidly after deposition, grain boundary α phase cannot form, and lamellar α grows rapidly inward from the grain boundaries. Compared to the middle and bottom deposition layers with numerous plate-like α phases, the microstructure at the top does not show significant α laths, but comparing it with the structure slightly below the top, as shown in Figure 10(b), indicates that with the continuous effect of the thermal cycle, these structures will form distinct Widmanstätten structure characteristics. The upper structure cools slowly from the β phase region to the α+β phase region, continuously undergoing a slow cooling process, causing continuously precipitated α phases to nucleate along the original β grain boundaries. Smaller α phases coalesce and grow into strip-like primary α phases; the lower the heat dissipation rate, the larger the phase region, as seen in Figure 10(c).

The middle and bottom parts of the TC4 titanium alloy CMT arc additive specimen experienced different degrees of thermal cycling, equivalent to different heat treatments, which caused significant changes in their microstructure. Due to the heat accumulation caused by multiple thermal cycles and the prolonged heating process, during slow cooling, the initial grain boundary primary α phase that nucleated on the original β grain boundaries turns to grow inward, forming phase-coherent, parallel elongated α lamellae structures, i.e., Widmanstätten structures, as shown in Figure 10(d). The existence of multiple thermal cycles in the additive manufacturing process leads to local coarsening of α grains, increasing in size.

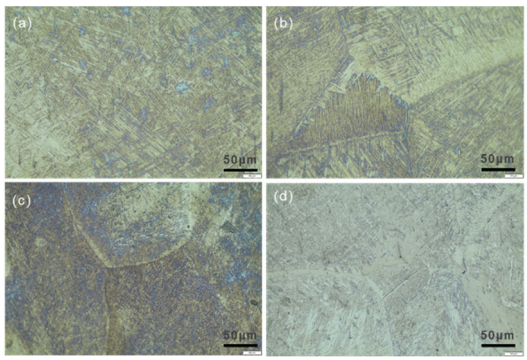

The top of the specimen cross-section; (b)The top of the specimen cross-section is compared to the top of the bottom; (c)Upper middle and upper cross-section of the specimen; (d)The bottom of the specimen cross-section

Figure 10. Microstructure of CMT additive manufactured metal

4. Summary

During the CMT arc additive manufacturing process of TC4 titanium alloy, as the number of deposited layers increases, the accumulation of heat leads to a decrease in the cooling rate, and the peak temperature of the molten pool will slightly increase. Throughout the multi-layer deposition process, the temperature curve on the substrate shows a cyclic state of peaks and troughs. As the deposition progresses, the temperature curve gradually smooths out, with the peak values gradually decreasing and the trough values gradually increasing, clearly indicating thermal accumulation.

During the single-pass multi-layer additive process, the equivalent stress of the deposition layers gradually decreases with the increase of the number of deposited layers. The accumulation of thermal stress caused by the addition and the stress cycles caused by multiple thermal cycles can increase the equivalent stress. However, the gradually decreasing cooling rate and remelting allow the interlayer stress to be well released, so there is no significant stress present after the additive specimen cools down, with the maximum equivalent stress value being 265MPa.

The microstructural characteristics of the CMT additive specimens include primary β phases spanning multiple deposition layers and growing in the direction of addition. With the increase in the number of stacked layers, the accumulation of heat input leads to the continuous growth of the primary β phase. The secondary phases in the specimen consist of a basketweave structure, primarily comprising α' martensite, α, and β phases. Among these, α' martensite is directly transformed from the primary β phase. Multiple reheating actions allow the secondary α phases to form through different pathways, with the protruding α phases being parallel to each other and having clear directionality. More basketweave structures form within the layers of the specimen, and a higher temperature gradient at the edges leads to the formation of more needle-like α' martensites.

References

[1] Wang Fuqiang, Wang Deyong. Study on the effects of heat-treatment on mechanical properties of TC4 titanium alloy sheets for aviation application [J]. Titanium Industry Progress, 2017, 34(02): 24-27.

[2] Yan S K, Song G L, Li Z X, et al. A state-of-the-art review on passivation and biofouling of Ti and its alloys in marine environments[J]. Journal of Materials Science and Technology, 2018, 34: 421–435.

[3] CHEN C, CHEN F, YANG Y, et al. Study on appearance and mechanical behavior of additively manufacturing of Ti–6Al–4V alloy by using cold metal transfer[J]. CIRP Journal of Manufacturing Science and Technology, 2021, 35: 250-258.

[4] Kobryn P A，Semiatin S L. The laser additive manufacture of Ti-6Al-4V[J]. Jom the Journal of the Minerals Metals and Materials Society, 2001, 53(9):40 -42.

[5] Yang W T , Long X Q . Special Corrosion Types of Titanium Alloy Used In Civil Aircraft[J]. Total Corrosion Control, 2008, 22(2):42

[6] Pustode M D, Raja V S, Paulose N. The stress-corrosion cracking susceptibility of near-titanium alloy IMI 834 in presence of hot salt[J]. Corrosion Science, 2014,82: 191

[7] Baufeld B, Biest O V D, Gault R. Microstructure of Ti-6Al-4V specimens produced by shaped metal deposition[J]. International Journal of Materials Research, 2009, 100 (11): 1536~1542.

[8] Baufeld B, Biest O V D, Gault R. Additive manufacturing of Ti-6Al-4V components by shaped metal deposition: Microstructure and mechanical properties[J]. Materials and Design, 2010, 31: 235~247.

[9] Wang F, Williams S, Paul Colegrove, et al. Microstructure and Mechanical Properties of Wire and Arc Additive Manufactured Ti-6Al-4V[J]. Metallurgical and Materials Transactions A, 2013, 44(2): 968~977.